Research Article | Vol. 30, No. 7 / 28 Mar 2022 / Optics Express 12014
Optics EXPRESS

Correction of a digital micromirror device lithography system for fabrication of a pixelated liquid crystal micropolarizer array

CHANG LIU,[1,5] SHIYUAN ZHANG,[2,3,5] YUQING LIU,[4] MEIYING LU,[1] WENHUI CAO,[1] LONG HUANG,[1] HAN ZHANG,[1] ZIFENG LU,[1] QUANQUAN MU,[2,3] AND HUA LIU[1,*]

[1]*Center for Advanced Optoelectronic Functional Materials Research and Key Laboratory for UV Emitting Materials and Technology of Ministry of Education, National Demonstration Center for Experimental Physics Education, Northeast Normal University, 5268 Renmin Street, Changchun 130024, China*
[2]*State Key Laboratory of Applied Optics, Changchun Institute of Optics, Fine Mechanics and Physics, Chinese Academy of Sciences, Changchun 130033, China*
[3]*Center of Material Science and Optoelectronics Engineering, University of Chinese Academy of Sciences, Beijing 100049, China*
[4]*State Key Laboratory of Integrated Optoelectronics, College of Electronic Science and Engineering, Jilin University, 2699 Qianjin Street, Changchun 130012, China*
[5]*These authors contributed equally to this work*
[*]*liuh146@nenu.edu.cn*

Abstract: The combination of a digital micromirror device (DMD) lithography system and a rotatable polarizer provides a simple and convenient method to achieve the pixelated liquid crystal micropolarizer (LCMP) array for polarization imaging. In this paper, two crucial problems restricting the high-precision fabrication of LCMP array are pointed out and settled: the dislocation of LCMP pixels caused by parallelism error of the rotating polarizer and the grid defect caused by the gap between micromirrors. After correction, the maximum deviation of the fabricated LCMP pixels was reduced from 3.23 μm to 0.11 μm and the grid defect is eliminated. The correction method reported here lays a good foundation for the fine processing of liquid crystal devices with arbitrary photoalignment structure by using the DMD system.

1. Introduction

In recent years, the use of polarimetry information is opening new possibilities in biomedicine [1], sample characterization [2,3], astronomy [4] and many other military fields [5]. This has prompted the proposal of different imaging polarimeters, which can be categorized as [6]: division of time polarimeter (DoTP), division of amplitude polarimeter (DoAmP), division of aperture polarimeter (DoAP), and division of focal-plane polarimeter (DoFP). DoFPs have been proved as the most ideal system for snapshot polarization imaging due to series advantages of compact structure, robust performance and portability [7,8].

A DoFP uses a pixelated micropolarizer array as the core element on the image sensor, where each pixel of both micropolarizer array and sensor is aligned. In commercial polarization cameras, like Sony IMX250MZR [9], an array of 0°, 45°, 90° and 135° pixelated wire-grid-polarizers is widely used, and the first three Stokes components (S_0, S_1, S_2) can be measured in the image. A pixelated wire-grid-polarizer array, typically with a grating period of 140 nm and duty cycle of 0.5 [10], is usually fabricated by electron beam lithography (EBL) and inductively coupled plasma-reactive ion etching (ICP-RIE). This requires nano-scale processing equipment and complicated processing procedures. Costly, and difficult to ensure its uniformity. Therefore, more and more researchers focus on the liquid crystal micropolarizer (LCMP) arrays [11–15].

#453800 https://doi.org/10.1364/OE.453800
Journal © 2022 Received 14 Jan 2022; revised 24 Feb 2022; accepted 24 Feb 2022; published 25 Mar 2022

Optics EXPRESS

Based on photoalignment technique, the processing accuracy can be effectively reduced from nano-scale down to micron-scale, and the fabrication process can also be significantly simplified.

Digital micromirror device (DMD) lithography has been considered as an advanced method for microstructure processing and three-dimension (3D) printing [16–18]. In recent years, it has also been studied to achieve different kinds of liquid crystal (LC) elements for optical field modulation via LC photoalignment technique [19,20]. Generally, the DMD lithography system is equipped with a rotatable linear polarizer (LP) to generate the linearly polarized light and LC photoalignment in different direction can be achieved. However, available commercial UV polarizers (from Thorlabs, Edmund, etc.) all have a parallelism error (usually about 1 - 20 arcmins [21]). Pixel dislocation in the LC element will be generated when the LP is rotated to different directions. Polarizers with better parallelism need to be customized with a long period and may cost dozens of times than the commercial products. In addition, the filling ratio of DMD is limited (about 92% [22]), an interval of about 1 μm exists between the micromirrors. Meanwhile, due to the limitation of projection objective aperture, the edges of each square micromirror shape are "smeared out" on the image plane. Therefore, under the illumination of incoherent light source (such as LED), every single micromirror will form an exposure pixel on the imaging plane whose energy is nearly Gaussian distribution [23,24]. These factors lead to grid defects in LC pixels. All the above-mentioned difficulties greatly reduce the quality of the LC device and limit further application of DMD lithography for LC photoalignment technology. Yet, few researchers have explored them in depth.

Our group has extensive experience in the fabrication of 2D and 3D microstructured devices via DMD lithography [25,26]. Aiming at the existing problems in fabricating LCMP mentioned above, a correction method is proposed in this paper for fine-tuning the LC cell using a precise piezoelectric stage. After correction, the maximum deviation of the fabricated LCMP pixels is reduced from 3.23 μm to 0.11 μm and the grid defect was eliminated. A 4-domain twisted liquid crystal micropolarizer (LCMP) array is fabricated successfully and modular DoFP system is built for polarization imaging experiments. The results indicate that the LCMP has good uniformity and optical performance after correction, which could meet the requirement of linear polarization imaging.

2. Fabrication of the LCMP array

The DMD lithography system is shown in Fig. 1(a). A LED light source (CBM-120-UV, from Luminus), with a central wavelength of 405 nm and full-width at half maximum (FWHM) of 15 nm, is collimated and evenly irradiated on the DMD. The DMD (DLP7000UV, Texas Instruments Inc.) used in the system is composed of 1024×768 micromirror array with single pixel pitch L of 13.68 μm. A nanoparticle linear polarizer (LPUV100, from Thorlabs) [21] is mounted on a rotating stage to generate linearly polarized light in different direction. The LC cell is fixed on a piezoelectric stage (P11.XYZ100S, from CoreMorrow) for correction.

The structure of LC cell is shown in Fig. 1(b). The inner surface of the top substrate is coated with polyimide (PI), which makes the LC molecules to align along the rubbing direction. The inner surface of the bottom substrate is coated with a photoalignment material SD1 [27] as the image plane of DMD lithography system. The two substrates are assembled together using sealant (NOA-68) mixed with 6.5 μm spacers. A thin film polarizer is attached to the outer surface of the top substrate with polarization axis parallel to the rubbing direction of the PI layer. When the LP is rotated to each design angle, the corresponding DMD mask will be projected onto the SD1 layer, as shown in Fig. 1(c) and (d). For each mask image, the exposure dose is 5 J/cm^2, then a pixelated photoalignment structure on SD1 layer is formed. Then, LC material is injected into the empty cell, and a twisted LCMP is formed. Each sub-pixel serves as a polarization rotator in different direction. Four adjacent sub-pixels are regarded as a superpixel.

Optics EXPRESS

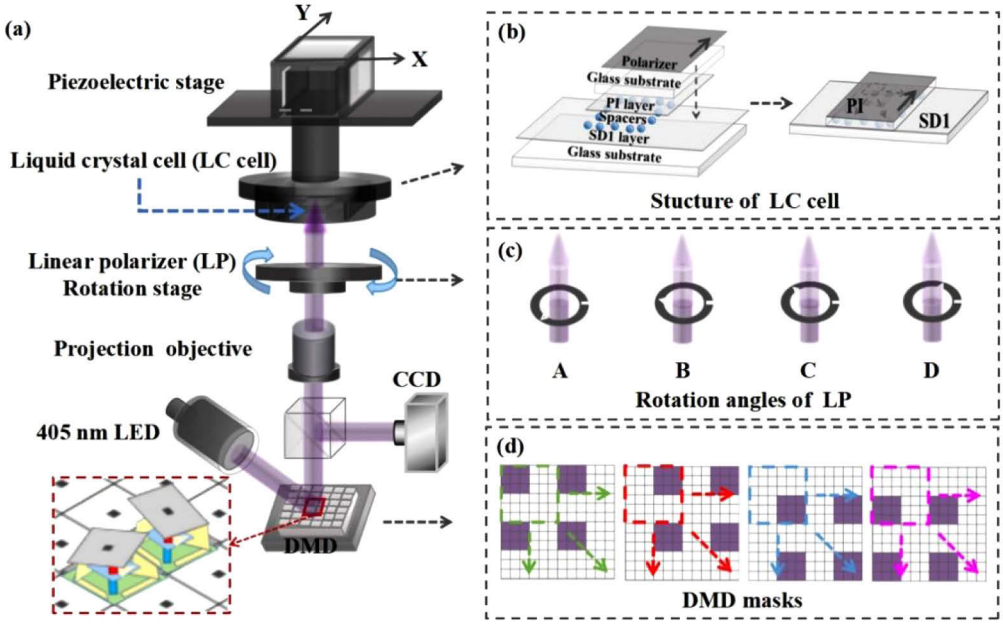

Fig. 1. (a) Schematic diagram of DMD lithography system. (b) Structure of liquid crystal cell. (c) The four angles of the linear polarizer (LP) for photoalignment. (d) DMD patterns of four sub-pixels in the LCMP array.

The mask patterns shown in the DMD are reduced by a projection lens and then exposed on the image plane. Each on-state DMD micromirror forms a single exposed pixel after being projected on the substrate. The exposure pixel size is defined as the product of the pixel size on the DMD array and the reciprocal of the magnification of the projection lens. The 2x objective (#59–875, from Edmond Optics) is used in our experiment, and the size of a single exposed pixel is 6.84 μm ($L/2 = 6.84$ μm). If an objective with a larger magnification is used instead, devices with smaller single exposed pixel can be fabricated.

A LCMP sample is fabricated directly using the method above, however, the structure of the sample is irregular. As shown in Fig. 2(a), there are grid defects in each sub-pixel and adjacent pixels overlap and dislocate. These disadvantages will severely limit the application of LCMP. The sub-pixel dislocation will cause it to fail to align with the pixel of the image sensor, and grid defects will lead to the decrease of the optical performance of the LCMP.

In order to find out the causes of these problems, a substrate coated with photoresist is used to replace the LC cell for photolithography exposure, and the structure shows in Fig. 2(b). Firstly, the overlapping of adjacent pixels in LCMP is caused by the dislocation of the DMD micromirror projection on the image plane. This should be due to the poor parallelism of the polarizer LP. A wedge angle between top and bottom substrates of the LP will lead to the dislocation of sub-pixels when the polarizer rotates to different angles. Second, each exposure pixel projected from the DMD micromirror and its boundaries within each pixel are clearly visible. This meanly caused by the limited DMD filling ratio. Gaps between the micromirrors cannot be exposed on the image plane. In addition, due to the diffraction characteristics of the projection objective, the edges of each square micromirror shape are “smeared out” on the image plane, which further aggravated the grid effect.

These two problems need to be solved in the preparation process of LCMP. Next, we will explain the mechanism of these problems and provides correction methods.

Optics EXPRESS

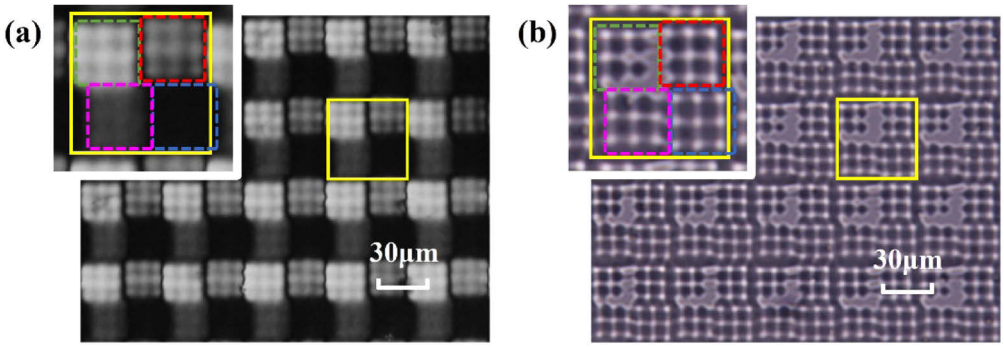

Fig. 2. Micrograph of (a) the LCMP array sample with severe sub-pixel dislocation and grid defect. (b) The pixel structure on photoresist, using 2x objective and combining 3*3 DMD exposed pixels.

3. Correction methods

In this paper, linearly polarized light with different polarization angles is produced by the rotating LP. It is necessary to calibrate the angle of LP first, as shown in Fig. 3(a). Since the orientation of SD1 is perpendicular to the direction of the 405 nm linearly polarized light, the orientation of LP should be perpendicular to the rubbing direction of PI. A polarizer (marked as P_0) is placed above LP and the transmission axis of P_0 is parallel to the friction direction of PI of the LC cell. Then, rotate LP by 360° and a power meter is employed to record the power at 5° intervals. The relation between the rotation angle of LP and power is shown in Fig. 3(b). Black dots represent measured values, and the red solid line is the fitting sin^2 curve followed Malus' Law with least-square method. The orientation of LP is fitted to be 124°. The four polarization angles of the designed LCMP are 22.5°, 67.5°, 112.5° and 157.5° (twist angles of ± 22.5°, ± 67.5°) [28]. Thus, the four rotation angles of LP are 146.5°, 191.5°, 236.5° and 281.5°, respectively.

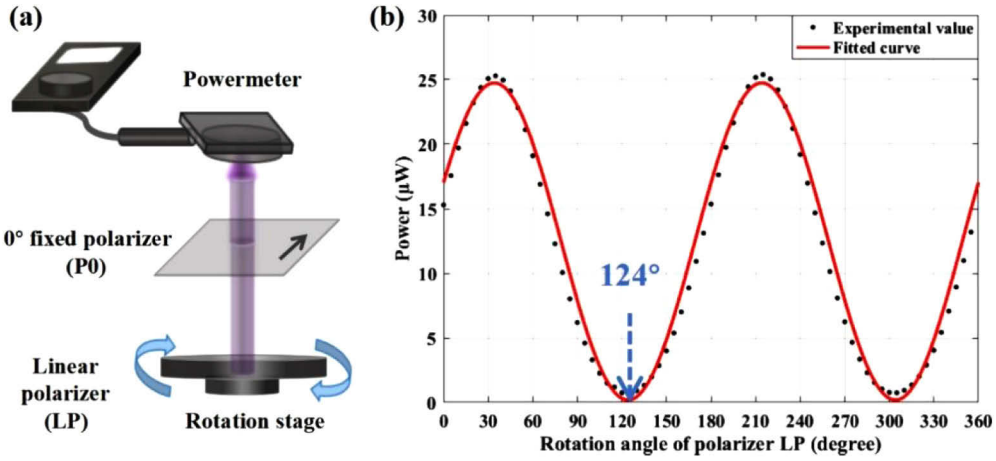

Fig. 3. (a) Calibration process of the polarizer LP orientation. (b) Malus' law is followed for sin^2 curve fitting and the orientation of LP is fitted to be 124°.

Optics EXPRESS

3.1. Dislocation

A commercial polarizer has a certain parallelism error, that is, a wedge angle exists between the top and bottom surface of the polarizer. This will cause the center position of the projected image to be offset when the LP is rotated to different directions, as shown in Fig. 4(a). The offset Δr is determined by the wedge angle α, refractive index n of the LP, and the distance from the top surface of the LP to the image plane Δz, which is shown by Eq. (1):

$$\Delta r = (n-1)\alpha\Delta z. \tag{1}$$

Since α, n and Δz are fixed, the offset value Δr is unchanged and its direction is consistent with the direction of LP wedge θ. When the LP rotates, the direction of LP wedge also changes, which causes the projected DMD image on the image plane rotate with the radius of Δr. Take the X, Y movement direction of the piezoelectric as the coordinate axis and use the offset rotation center as the coordinate origin. Assuming the initial azimuth of LP wedge is θ_0, the projection component of the center offset $(x_0,\ y_0)$ of the projected image in this coordinate system is:

$$\begin{aligned} x_0 &= \Delta r \cos\theta_0 \\ y_0 &= \Delta r \sin\theta_0. \end{aligned} \tag{2}$$

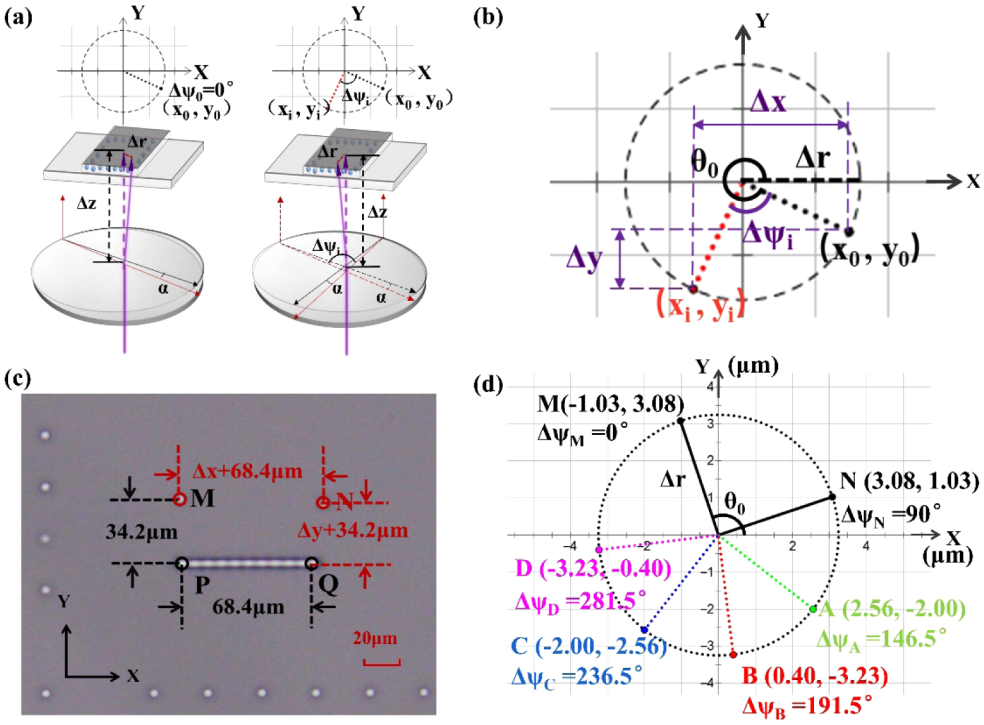

Fig. 4. (a) Diagram of the dislocation caused by the rotation of the LP wedge. (b) The relative distance Δx, Δy between (x_i, y_i) and (x_0, y_0). (c) The exposure points are separated for easy measurement under the microscope. (d) The positions of dislocations at four LP angles.

The initial position of the LP on the rotation stage is set as $\psi_0 = 0°$. When the LP is rotated by an angle $\Delta\psi_i$ and a same image is projected, as is shown in Fig. 4(b). The projected component

Optics EXPRESS

of the new image center offset $(x_i,\ y_i)$ is:

$$\begin{aligned} x_i &= \Delta r \cos(\theta_0 + \Delta\psi_i) \\ y_i &= \Delta r \sin(\theta_0 + \Delta\psi_i). \end{aligned} \tag{3}$$

The distance Δx and Δy between $(x_i,\ y_i)$ and $(x_0,\ y_0)$ can be measured and the center offset $(x_i,\ y_i)$ can be solved:

$$\begin{aligned} x_i &= x_0 + \Delta x = x_0 \cos\Delta\psi_i - y_0 \sin\Delta\psi_i \\ y_i &= y_0 + \Delta y = x_0 \sin\Delta\psi_i + y_0 \cos\Delta\psi_i. \end{aligned} \tag{4}$$

According to Eq. (4), just take two non-coincident points and measure the relative distance $\Delta x,\ \Delta y$ between the two points, $(x_0,\ y_0)$ can be determined. Then, Δr and θ_0 can be calculated according to Eq. (2), and the offset components of four polarization angles are obtained. Finally, the dislocations at the four polarization angles are compensated by the preset motion of the piezoelectric stage.

In the experiment, the single-pixel point M is exposed at the initial position of LP $\psi_0 = 0°,\ (\Delta\psi_M = 0°)$, and the single-pixel point N is exposed by rotating the LP to any angle (the position where $\Delta\psi_N = 90°$ is selected in the experiment). Since the two points are very close to each other and cannot be distinguished, point M and point N are separated for measurement in the experiment. A line segment PQ of 10 pixels (68.4 μm in length) and two rows of exposure points perpendicular to each other are added as coordinate axes to facilitate the alignment of direction. PQ and coordinate axes are exposed at the initial position of LP $\psi_0 = 0°$. Point M and point N are 5 pixels above point P and point Q, respectively. The measurement is taken using a microscope (Olympus BX53M), as shown in Fig. 4(c). The measured and calculated Δx, Δy obtained by extracting the position of the pixel have an error within ± 0.10 μm. Consequently, the maximum error of Δr is about ± 0.10 μm when the angle between the two points is 90°. According to the measurement, Δx is 4.11 ± 0.10 μm and Δy is −2.05 ± 0.10 μm.

By substituting Δx and Δy into the Eq. (4), the coordinates of point M are −1.03 ± 0.03 and 3.08 ± 0.09, the coordinates of point N are 3.08 ± 0.09 and 1.03 ± 0.03, respectively. The size of Δr is about 3.24 ± 0.10 μm; and θ_0 is about 108.5°. According to the values of Δr and θ_0 and the four LP angles of $\Delta\psi_A = 146.5°$, $\Delta\psi_B = 191.5°$, $\Delta\psi_C = 236.5°$ and $\Delta\psi_D = 281.5°$ the offset components along the X and Y directions of piezoelectric motion at the four LP angles A, B, C and D in the experiment are calculated, as shown in Fig. 4(d). The horizontal and vertical coordinates of each point represent the distance to be compensated for the dislocation along the X and Y directions of the piezoelectric stage. Since the maximum error of Δr is ± 0.1 μm, each point has a corresponding error. After calculation, A is at (2.56 ± 0.08, −2.00 ± 0.06), B is at (0.40 ± 0.01, −3.23 ± 0.01), C is at (−2.00 ± 0.06, −2.56 ± 0.08) and D is at (−3.23 ± 0.01, −0.40 ± 0.01). It can be seen that the maximum dislocation along the X and Y directions is 3.23 ± 0.01 μm. The offset components along the X and Y directions of the four sub-pixels of LCMP are programmed and input the piezoelectric stage for precise displacement. By this means, the dislocations of LCMP sub-pixels are improved.

3.2. Grid defect

DMD consists of many micromirrors. Each of the DMD micromirror is independent and an interval of about 1 μm exists between the micromirrors. Meanwhile, due to the limitation of projection objective aperture, the high-frequency part of the diffractive light from the “on"-state micromirrors is removed. Therefore, under the illumination of incoherent light source (such as LED), every single micromirror will form an exposure pixel on the imaging plane. Therefore, there will be grid defect in every single pixel of the LCMP array. A superposing exposure method is proposed to eliminate the grid defect.

Optics EXPRESS

In this experiment, a 2x objective (#59–875, from Edmond Optics) is used. The illumination profile from a single micromirror $S(x, y)$ in row m and column n is expected to be a convolution between the micromirror shape $M(x, y)$ and the point-spread function $PSF(x, y)$, as shown in Eq. (5). This convolution will tend to "smear out" the square mirror shape.

$$S(x, y) = M(x, y) * PSF(x, y). \tag{5}$$

The energy of the exposed pixels projected by DMD micromirrors in the range of $i * j$ ($0 < i \leq 1024,\ 0 < j \leq 768$) can be expressed as Eq. (6):

$$I_{sum} = \sum_{m=0}^{i} \sum_{n=0}^{j} P_{m,n} S(x + mh, y + nh), \tag{6}$$

where $P_{m,n}$ is the intensity coefficient related to exposure time; h is equal to the size of a single exposed pixel ($h = L/2$). In Fig. 5(a-i), it shows the energy distribution on the cross section in X direction of an LCMP sub-pixel generated by $k * k$ DMD pixels ($i = k, j = k$). To eliminate the grid defect showed in Fig. 5(b-i), it is necessary to compensate for the energy in the gap of adjacent DMD exposed pixels. Here, the piezoelectric stage is used to drive the LC cell, allowing the designed mask patterns to be superposed on the gap between adjacent exposed pixels.

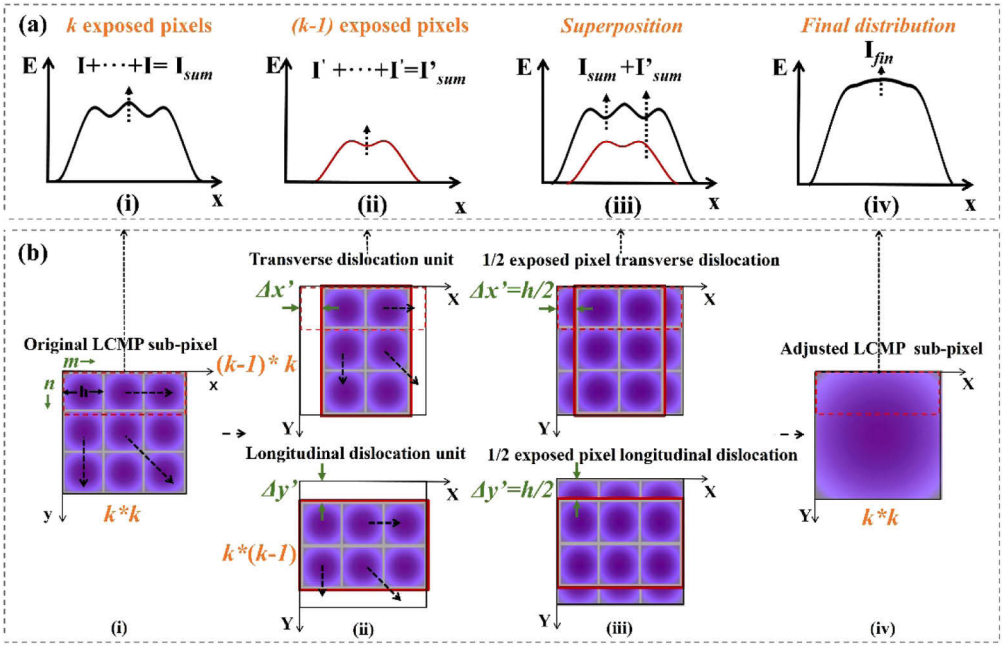

Fig. 5. Correction method for grid defect. (a) Schematic draw of the cross-section energy distribution in the X direction of an LCMP sub-pixel. (b) Schematic draw of the process of the correction method for grid defect. 1/2 exposed pixel superposition in X and Y direction on the original $k * k$ DMD exposed pixels.

After the distances of Δx and Δy ($0<\Delta x'<h, 0<\Delta y'<h$) are moved along the X and Y directions, respectively, the sum energy of exposed pixels is given by Eq (7):

$$I'_{sum} = \sum_{m=0}^{i} \sum_{n=0}^{j} P'_{m,n} S(x + mh + \Delta x', y + nh + \Delta y'). \tag{7}$$

Optics EXPRESS

Here $\Delta x'$ and $\Delta y'$ are equal to $h/2$, $P'_{m,n}$ is the intensity coefficient. The energy distribution on the X-direction cross section of the transverse dislocation unit is shown in Fig. 5(a-ii). According to Eq. (7), a mask pattern of $(k-1) * k$ DMD pixels is designed and exposed at the dislocation of 1/2 exposed pixel along the X direction and a mask pattern of $k * (k-1)$ pixels is designed and exposed at the dislocation of 1/2 exposed pixel along the Y direction, as showed in Fig. 5(b-ii) and (b-iii).

Because we use incoherent source (LED) for illumination, the flux-density contribution of exposed pixels is additive, as shown in Fig. 5(a-iii). In this way, the final energy distribution in the range of $k * k$ DMD exposed pixels is shown in Eq. (8):

$$I_{fin} = I_{sum} + I'_{sum}. \tag{8}$$

By controlling the exposure time, the energy of the superposing exposure in the gap is the same as the energy at the center of the single exposed pixel. From the energy distribution on the X-direction cross section, as shown in Fig. 5(a-iv), the gap between adjacent exposed pixels can be effectively filled after superimposed exposure. By this means, the grid defect in LCMP sub-pixel is eliminated, as shown in Fig. 5(b-iv).

3.3. Fabrication and characterization of the LCMP array after correction

A LCMP array is fabricated successfully using the correction method above, and a photo of the LCMP array device shows in Fig. 6(a). A 2x objective is used here and 13 * 13 DMD pixels are combined into one sub-pixel. The LCMP array contains 39 * 29 superpixels in total. Since the size of a DMD exposed pixel is 6.84 μm (13.68 μm / 2), the pitch of a sub-pixel is 88.92 μm (6.84 μm * 13). The four sub-pixels (named A, B, C and D) are exposed at 146.5°, 191.5°, 236.5° and 281.5°, respectively. Thus, the photoalignment on SD1 layer is supposed to be 22.5°, 67.5°, 112.5° and 157.5°. Each sub-pixel serves as a polarization rotator, twist angles of ± 22.5°, ± 67.5°.

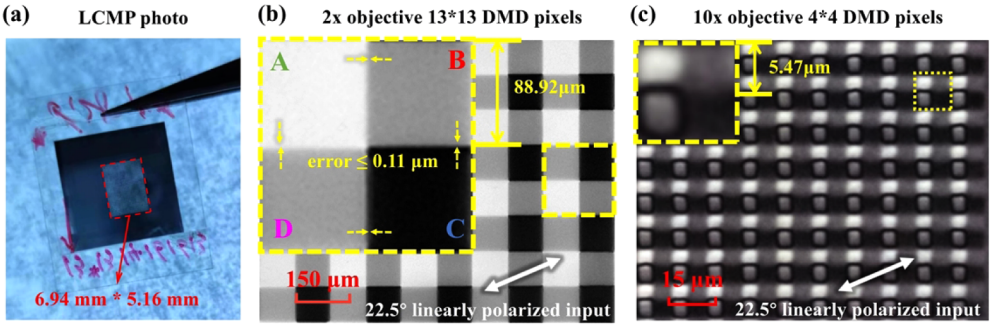

Fig. 6. (a) Photo of the LCMP. Its size is 6.94 mm*5.16 mm. (b) Micrograph of the LCMP array with a sub-pixel pitch of 88.92 μm using 2x objective and combining 13*13 DMD exposed pixels. (c) Micrograph of the LCMP array with a sub-pixel pitch of 5.47 μm using 10x objective and combining 4*4 DMD exposed pixels. The dislocation and grid defect are improved after correction. Both of two LCMP arrays are illuminated by 22.5° linearly polarized light.

Dislocation correction is carried out for each sub-pixel according to the direction and distance marked in Fig. 4(d). Grid defect is also corrected using the process showed in Fig. 5(b). A mask pattern of 12*13 DMD pixels is designed and exposed to get the transverse dislocation single-polarization unit and a mask pattern of 13*12 DMD pixels is exposed to get the longitudinal dislocation single-polarization unit. For each sub-pixel, the exposure dose should be added up to

Optics EXPRESS

5 J/cm^2 (exposure time of about 80 s in our system). We the exposure time. The adjusted exposure time is divided into 40 s for the original sub-pixel and 20 s each for the transverse and longitudinal dislocation units respectively. The LCMP is illuminated by 22.5° linearly polarized light and a micrograph is captured as shown in Fig. 6(b). After correction, the maximum dislocation of the device in X and Y directions is corrected from 3.23 μm to less than 0.11 μm (including the round-off error in calculation of about 0.01 μm and the measurement error of about 0.1 μm in the microscope) and the grid defect is eliminated.

We also fabricated a LCMP sample with smaller pixel, using a 10x objective (#59–877, from Edmond Optics) and combining 4*4 DMD pixels into one sub-pixel for photoalignment exposure. The LCMP array with sub-pixel pitch of about 5.47 μm (13.68 μm / 10 × 4) have been achieved successfully after the correction of the dislocation and grid defect. The sample is illuminated by 22.5° linearly polarized light and a micrograph is captured as shown in Fig. 6(c). It also shows a regular structure. It can be seen that the correction method proposed in this paper is of great significance for the development of micropolarizer arrays based on LC photoalignment technique.

4. Polarization imaging experiment

A modular DoFP system is built for principle polarization imaging experiments. The LCMP array should be aligned with CMOS array and calibrated first [29]. As shown in Fig. 7(a), A white LED combined with a 632.8 nm bandpass filter (FWHM of 10 nm) and a collimating lens is used for illumination. Indeed, twisted LC cannot provide strictly consistent polarization rotation angle for different wavelength. While in this paper, due to the use of large LC material, Mauguin condition is satisfied in most visible wavelengths [28]. Thus, there wouldn't be significant difference in

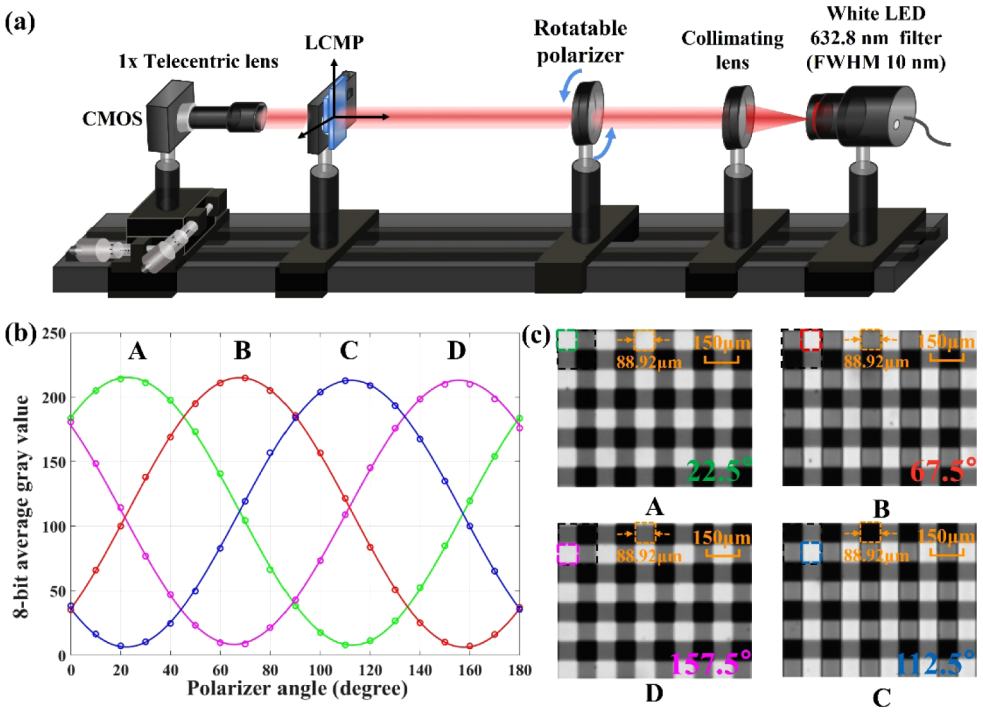

Fig. 7. Schematic diagram of optical setup for aligned with CMOS array and calibrate (a) The average gray value of the four sub-pixels changed with the polarization direction of the incident light. (b) The internal structure of LCMP recorded by CMOS when the analyzer is at the four angles of 22.5°, 67.5°, 112.5° and 157.5°.

Optics EXPRESS

the results of polarization imaging between broadband and a single wavelength. The pixel size of the CMOS camera is 5.2 μm, and the sub-pixel with a pitch of 88.92 μm designed in this paper roughly corresponds to 17 * 17 (88.4 μm * 88.4 μm) pixels in the CMOS camera. Using a double telecentric lens (F/12) as a relay lens, the LCMP array can be imaged on the focal plane of the camera. The LCMP is illuminated with a series of uniform linearly polarized state beams generated by rotating a polarizer from 0° to 180° at intervals of 10°. The gray value corresponding to the sub-pixels are extracted. The average gray value curve with the of rotation angle is shown in Fig. 7(b). When the polarizer is at the four angles of 22.5°, 67.5°, 112.5° and 157.5°, the internal structure image of the LCMP array recorded by the CMOS is shown in the Fig. 7(c).

The extinction ratio can be used to evaluate the polarization performance of LCMP. The extinction ratio [30] calculation of images extracted by CMOS is as follows:

$$T = \frac{G_{\max}}{G_{\min}}. \tag{9}$$

where, G_{max} and G_{min} respectively represent the average maximum and minimum gray values of the sub-pixels with the same twist angle, respectively. The angle corresponding to the maximum gray value and the minimum gray value differs by 90°. According to the numerical calculation in Fig. 7(a), the extinction ratios T of the four sub-pixels are 34.12, 27.24, 24.47 and 32.76, respectively.

In order to verify the performance of the fabricated LCMP, polarization imaging experiment was carried out. The optical setup is shown in Fig. 8(a). A 0.32x double telecentric lens (F/8)

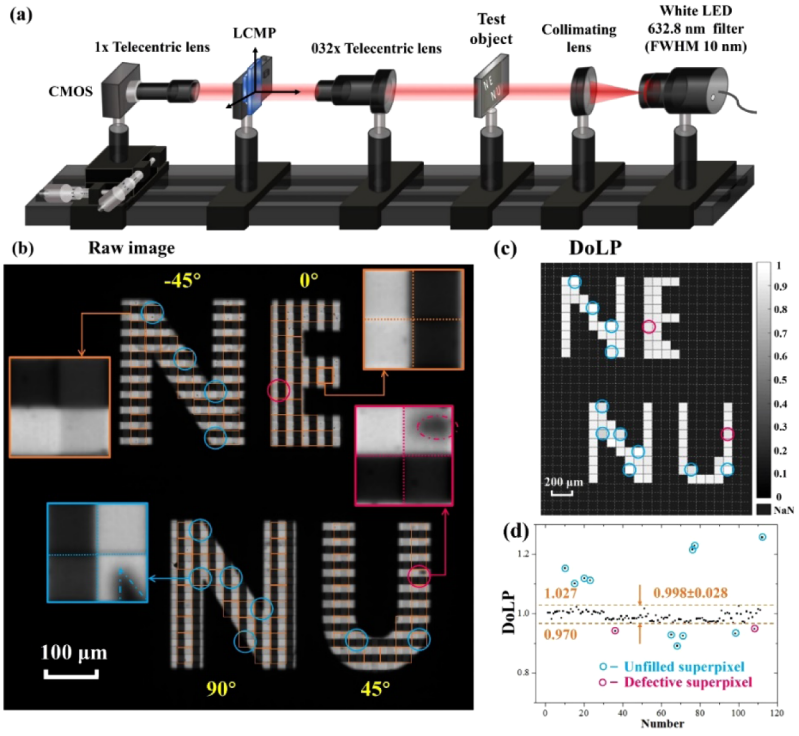

Fig. 8. (a) Schematic diagram of a modular DoFP system for polarization imaging (b) Raw image of the test object captured by CMOS. (c) DoLP pseudo-color image of the test object. (d) A fitting figure of the numerical distribution of DoLP.

Optics EXPRESS

is used as an image objective in front of the LCMP. The test object is the perforated aluminum plate. The perforated part consists of four letters "**N**", "**E**", "**N**" and "**U**" covered with a polarizer different orientation, respectively (polarization axis of in −45°, 0°, 45° and 90°). The raw image captured by a CMOS camera is shown in Fig. 8(b). The part of each letter that occupies an entire superpixel is extracted (marked with an orange box). The data at the edge of each hole and the opaque part were removed in the results. The degree of linear polarization (DoLP) [31] is calculated and its value distribution of each superpixel are shown in Fig. 8(c). Superpixels where DoLP significantly deviate from 1 can be attributed to the opaque edges (blue circles) and defects on the polarizer (pink circles) that cause abnormal intensity differences and lead to calculation errors [32]. The values of DoLP are in the range of 0.998 ± 0.028. It proves that the uniformity of polarization imaging by using the fabricated LCMP array is good. Therefore, it is verified that the fabricated LCMP by our method has achieved an excellent result, and it holds great promise for developing a cost-effective polarization camera.

5. Conclusion

DMD lithography system combined with a rotatable linear polarizer is a flexible and effective method for LC photoalignment. However, dislocation among the exposure patterns in all directions and the grid defect of the sub-pixels will have a great impact on the precise processing and performance test of the pixelated LC devices. Focusing on the fabrication of LCMP array, we introduced the reasons for these problems and proposed solutions for micro-displacement correction and superposition exposure compensation using the piezoelectric stage. Finally, the LCMP array without dislocation and grid defect is fabricated. The polarization imaging test have shown good results. By replacing the projection lens with a larger multiple, LCMP array with smaller pixels has potential to be fabricated for integrating directly into a polarization camera. The correction method presented in this paper plays an important role in the precision process of LC photoalignment using DMD system.

Funding. Jilin Scientifific and Technological Development Program (20190302049GX); National Natural Science Foundation of China (61875036).

Disclosures. The authors declare no conflicts of interest.

Data availability. Data underlying the results presented in this paper are not publicly available at this time but may be obtained from the authors upon reasonable request.

References

1. M. Garcia, C. Edmiston, R. Marinov, A. Vail, and V. Gruev, "Bio-inspired color-polarization imager for real-time in situ imaging," Optica **4**(10), 1263–1271 (2017).
2. M. Novak, J. Millerd, N. Brock, M. North-Morris, J. Hayes, and J. Wyant, "Analysis of a micropolarizer array-based simultaneous phase-shifting interferometer," Appl. Opt. **44**(32), 6861–6868 (2005).
3. N. Brock, B. Kimbrough, and J. Millerd, "A pixelated polarizer-based camera for instantaneous interferometric measurements," Proc. SPIE **8160**, 81600W (2011).
4. G. C. Giakos, "Multifusion, Multispectral, Optical Polarimetric Imaging Sensing Principles," IEEE Trans. Instrum. Meas. **55**(5), 1628–1633 (2006).
5. J. S. Tyo, M. P. Rowe, E. N. Pugh Jr., and N. Engheta, "Target detection in optically scattering media by polarization-difference imaging," Appl. Opt. **35**(11), 1855–1870 (1996).
6. J. S. Tyo, D. L. Goldstein, D. B. Chenault, and J. A. Shaw, "Review of passive imaging polarimetry for remote sensing applications," Appl. Opt. **45**(22), 5453–5469 (2006).
7. N. Gu, B. Yao, L. Huang, and C. Rao, "Design and Analysis of a Novel Compact and Simultaneous Polarimeter for Complete Stokes Polarization Imaging with a Piece of Encoded Birefringent Crystal and a Micropolarizer Array," IEEE Photonics J. **10**(2), 1–12 (2018).
8. M. Kulkarni and V. Gruev, "Integrated spectral-polarization imaging sensor with aluminum nanowire polarization filters," Opt. Express **20**(21), 22997–23012 (2012).
9. https://thinklucid.com/product/phoenix-5-0-mp-polarized-model/
10. Z. Zhang, F. Dong, T. Cheng, K. Qiu, Q. Zhang, W. Chu, and X. Wu, "Nano-fabricated pixelated micropolarizer array for visible imaging polarimetry," Rev. Sci. Instrum. **85**(10), 105002 (2014).
11. X. Zhao, A. Bermak, F. Boussaid, T. Du, and V. G. Chigrinov, "High-resolution photoaligned liquid-crystal micropolarizer array for polarization imaging in visible spectrum," Opt. Lett. **34**(23), 3619–3621 (2009).

Optics EXPRESS

12. X. Zhao, A. Bermak, F. Boussaid, and V. G. Chigrinov, "Liquid-crystal micropolarimeter array for full Stokes polarization imaging in visible spectrum," Opt. Express **18**(17), 17776–17787 (2010).
13. X. Zhao, F. Boussaid, A. Bermak, and V. G. Chigrinov, "High-resolution thin "guest-host" micropolarizer arrays for visible imaging polarimetry," Opt. Express **19**(6), 5565–5573 (2011).
14. G. Myhre, W.-L. Hsu, A. Peinado, C. LaCasse, N. Brock, R. A. Chipman, and S. Pau, "Liquid crystal polymer full-stokes division of focal plane polarimeter," Opt. Express **20**(25), 27393–27409 (2012).
15. W.-L. Hsu, G. Myhre, K. Balakrishnan, N. Brock, M. Ibn-Elhaj, and S. Pau, "Full-Stokes imaging polarimeter using an array of elliptical polarizer," Opt. Express **22**(3), 3063–3074 (2014).
16. H. Zhuang, W. Feng, L. Jiang, Y. Wang, and Z. Liu, "Assessment of spinal tumor treatment using implanted 3D-printed vertebral bodies with robotic stereotactic radiotherapy," The Innovation **1**(2), 100040 (2020).
17. D. Wang, J. Zhang, Q. Liu, B. Chen, and G. Jiang, "3D printing challenges in enabling rapid response to public health emergencies," The Innovation **1**(3), 100056 (2020).
18. X. Zheng, P. Kunwar, and P. Soman, "Hydrogel-Based Diffractive Optical Elements (hDOEs) Using Rapid Digital Photopatterning," Adv. Optical Mater. **9**(2), 2001217 (2021).
19. H. Wu, W. Hu, H. Hu, X. Lin, G. Zhu, J. W. Choi, and Y. Lu, "Arbitrary photo-patterning in liquid crystal alignments using DMD based lithography system," Opt. Express **20**(15), 16684–16689 (2012).
20. P. Chen, S. Ge, D. Wei, B. Wei, G. Cui, W. Hu, and Y. Lu, "Digitalized Geometric Phases for Parallel Optical Spin and Orbital Angular Momentum Encoding," ACS Photonics **4**(6), 1333–1338 (2017).
21. https://www.thorlabschina.cn/newgrouppage9.cfm?objectgroup_id=752
22. https://www.ti.com/product/DLP7000UV
23. C. Sun, N. Fang, D. Wu, and X. Zhang, "Projection micro-stereolithography using digital micro-mirror dynamic mask," Sens. Actuators A Phys. **121**(1), 113–120 (2005).
24. G. R. V. Kumar and K. Sayanagi, "Measurement of Optical Transfer Function by its Moments*," J. Opt. Soc. Am. **58**(10), 1369–1374 (1968).
25. Y. Zhang, J. Luo, Z. Xiong, H. Liu, L. Wang, Y. Gu, Z. Lu, and J. Huang, "User-defined microstructures array fabricated by DMD based multistep lithography with dose modulation," Opt. Express **27**(22), 31956–31966 (2019).
26. S. Guo, Z. Lu, Z. Xiong, L. Huang, and J. Li, "Lithographic pattern quality enhancement of DMD lithography with spatiotemporal modulated technology," Opt. Lett. **46**(6), 1377–1380 (2021).
27. M.-C. Tseng, O. Yaroshchuk, T. Bidna, A. K. Srivastava, V. Chigrinov, and H.-S. Kwok, "Strengthening of liquid crystal photoalignment on azo dye films: passivation by reactive mesogens," RSC Adv. **6**(53), 48181–48188 (2016).
28. S. Zhang, C. Liu, Z. Sun, Q. Mu, J. Campos, H. Liu, X. Zhang, D. Li, and Q. Wang, "4-domain twisted liquid crystal micropolarizer array for visible linear polarization imaging," Opt. Express **29**(26), 43226–43240 (2021).
29. S. B. Powell and V. Gruev, "Calibration methods for division-of-focal-plane polarimeters," Opt. Express **21**(18), 21040–21055 (2013).
30. G. Myhre, A. Sayyad, and S. Pau, "Patterned color liquid crystal polymer polarizers," Opt. Express **18**(26), 27777–27786 (2010).
31. V. Gruev, R. Perkins, and T. York, "CCD polarization imaging sensor with aluminum nanowire optical filters," Opt. Express **18**(18), 19087–19094 (2010).
32. R. A. Chipman, W. -S. T. Lam, and G. Young, *Polarized Light and Optical Systems* (Chemical Rubber Company, 2018), Chap. 7.